Available online at www.eccomasproceedia.org
Eccomas Proceedia SMART (2023) 1447-1457

ECCOMAS
Proceedia

X ECCOMAS Thematic Conference on Smart Structures and Materials
SMART 2023
D.A. Saravanos, A. Benjeddou, N. Chrysochoidis and T. Theodosiou (Eds)

# DYNAMICAL BEHAVIOR OF A SHAPE MEMORY ALLOY HOLED PLATE AND INVESTIGATION OF THE DAMPING EFFECT

**F. THIEBAUD*** **and T. BEN ZINEB***

* Université de Lorraine, CNRS, Arts et Métiers ParisTech, LEM3, F-54000, Nancy, France
e-mail: frederic.thiebaud@univ-lorraine.fr, web page: http://www.lem3.univ-lorraine.fr/

**Abstract.** Shape memory alloys (SMAs) are good candidates as passive dampers. In order to develop the use of these alloys in structural vibrations control, the dynamical response of a NiTi holed disc and its damping effect is investigated. At first, the material superelastic behavior is characterized in order to build a numerical tool based on a phenomenological SMA model implemented in the finite element code Abaqus ©. This numerical tool allows to identify the range of the amplitude of vibrations where the superelastic effect is on, without leading to the damage of the disc. A dynamic mechanical analysis (DMA) versus many parameters is performed on the disc which leads to the investigation of its damping effect by using the equivalent complex stiffness approach. The non linear behavior of the disc is shown and its damping performance is finally discussed.

**Key words:** Shape Memory Alloys, Superelastic behavior, Damping effect, Dynamic Mechanical analysis, Equivalent complex stiffness.

## 1 INTRODUCTION

Shape memory alloys (SMAs) are widely studied as smart materials because of their potentiality to be used as dampers, absorbers or actuators elements. For damping applications, an understanding of the material dynamic behavior is needed. The damping properties of SMAs are induced by the dissipated energy linked to the martensite transformation between the mother phase called austenite (A) and the product phase called martensite (M). In this case, the SMA elements are used as absorbers mainly for seismic applications. One can cite the studies leaded by Bono and Tirelli [1], Tirelli et al. [2], Dolce et al. [3], Piedboeuf et al. [4] and Fang et al. [5] for example. Moreover, a review about ths topic was proposed by Janke et al. [6].
This interest leads to many studies about the modelisation of the dynamical behavior of SMAs and their damping effect as it is mentioned in the studies of Gandhi and Wolons [7], Collet et al. [8] and Amarante Dos Santos and Cismasiu [9]. More recently, the shape memory effect was investigated for damping applications too as it is mentioned in Megdiche et al. [10].
The state of the art shows that actually most part of the work focuses on the modelisation of the damping effect and neither has there been much work on the study on original dampers


Peer-review under responsibility of the organizing committee of SMART 2023.
doi: 10.7712/150123.9916.445188

designed from superelastic SMA although one can cite the work leaded by Fang et al. [5] on Belleville washers or Mirzaeifar et al. [11] on helical springs.
Thus, In this paper we present the dynamical characterization and the evaluation of the damping effect of an innovative superelastic damper designed as a holed disc built in NiTi.
In the first part, the geometrical characteristics of the damper and the identification of the SMA thermomechanical behavior under a quasi-static loading are presented. To do this, tensile tests at room temperature and quasi-static rates are leaded. In the second part, a numerical tool is designed to predict the range of the amplitude of vibrations where the superelastic is activated. This involves to identify the superelastic parameters of the NiTi SMA. Thus, numerical simulations of the cyclic tensile test of the damper are leaded and the amplitude range is identified. In the third part, dynamic mechanical analysis (DMA) are carried out to evaluate the damping effect of the studied structure as function of many parameters such as the amplitude of vibration (in the considering range), the frequency and a static pre-displacement. The damping effect is here modeled by the innovative concept of the equivalent complex stiffness previously presented in Thiebaud and Ben Zineb [12].
The results clearly show that there is an optimized set of parameters which improve the damping effect of the structure.

## 2 STATIC CHARACTERIZATION OF THE SMA BEHAVIOR AND THE DAMPER RESPONSE

### 2.1 Design of the damper

The design of the damper studied in this paper is classically used as a springer in vibrating pots. It is a disc with many oblong holes, built by wirecut electric discharge process in a main NiTi superelastic plate with a thickness about 0.6 mm and provided by Nimesis©. The design of the damper and its dimensions are specified in the figure 1.

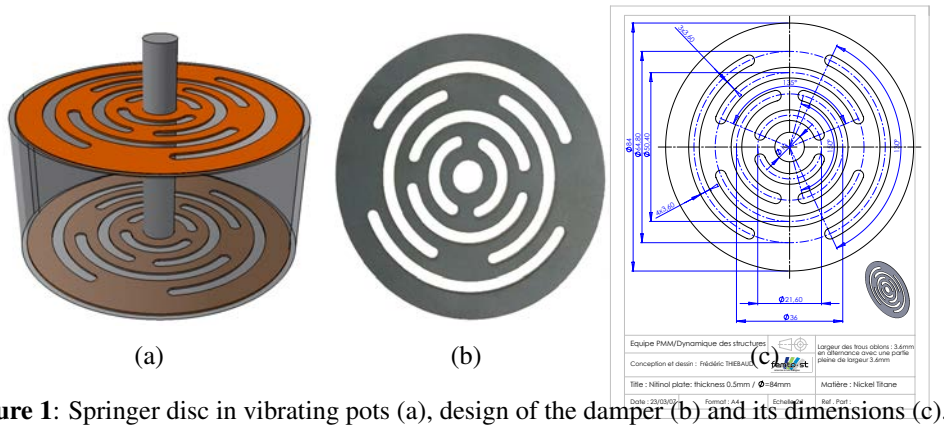


**Figure 1**: Springer disc in vibrating pots (a), design of the damper (b) and its dimensions (c).

## 2.2 Superelastic behavior of the NiTi SMA

Tensile samples are cut in the main plate with a standard shape in order to lead tensile tests. A destructive tensile test and a cyclic test at room temperature with a quasi-static rate are performed to identify the characteristic transformation stress (figure 2). Their width is about 3 mm and their thickness is about 0.6 mm. A tensile machine Zwick/Roell with a capacity 100 kN is used and the strain is locally measured with a clipon extensometer. The curves given in the figure 2 show that the forward transformation starts at the stress $\sigma^s_{AM}$ = 475 MPa and finishes at the stress $\sigma^f_{AM}$ = 550 MPa. The fracture stress is measured around 1000 MPa. Consequently, in order to prevent the fatigue effects during the use of the damper and thus its break, it's preferable to stay at a local stress in the range of 475 - 550 MPa.

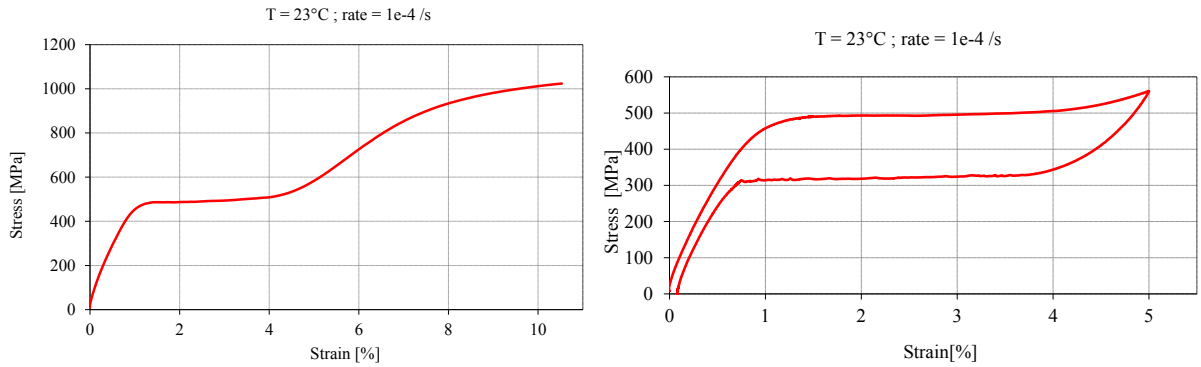


(a) (b)

**Figure 2**: Tensile tests on NiTi SMA.

## 2.3 Numerical prediction of the mechanical behavior of the damper

In order to activate superelastic behavior and thus the damping effect in the disc, it is important to estimate the displacement on which the forward martensitic transformation starts. Likewise, it is important to estimate the maximum admissible displacement in order to prevent the break of the disc. Both estimations are identified by static numerical simulations using a three dimensional phenomenological model.

### 2.3.1 Identification of the material parameters

As it is shown in the figure 2, the SMA behavior considered in this study is induced by the martensitic transformation in the SMA. In stress-free state, the SMA is supposed to be fully austenitic. During the load, the phase can change locally to martensite. The phenomenological model used in this paper is motivated by the work of Peultier et al. [13] and improved by Chemisky and Duval [14]. The reader can refer to these references to get more information about the model.

Twenty parameters are required for this phenomenological model. Implemented in Abaqus© via an UMAT subroutine, a numerical cyclic tensile test is performed in order to fit the experimental curve given in the figure 2(b). The result of this simulation shows a good correlation between both experimental and numerical results (figure 3). Finally, the parameters of the model are given in the table 1.

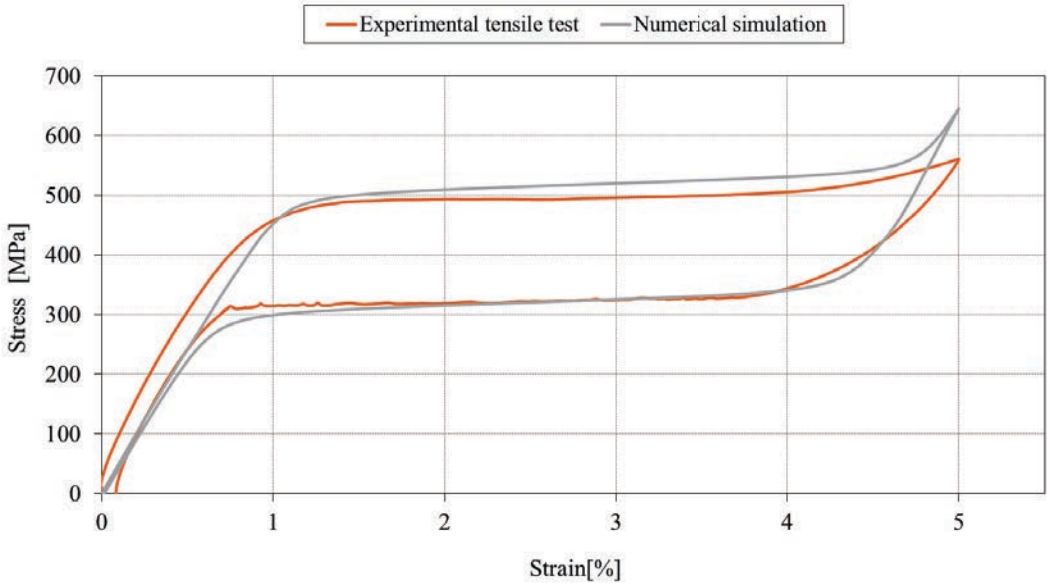


**Figure 3**: Tensile tests on NiTi tensile samples.

**Table 1**: Material parameters

| $E$ (MPa) | $\nu$ | $\alpha$ (/K) | $\varepsilon^{tr}_{max}$ | $\varepsilon^{tr}_{mart}$ |
|---|---|---|---|---|
| 50000 | 0.3 | 0 | 0.035 | 0.05 |
| $R_f$ | $F^{max}_{et}$ | $H_f$ | $H_{eps}$ | $H_{twin}$ |
| 0.6 | 120 | 1 | 2500 | 40000 |
| $\varepsilon^{c}_{max}$ | $b^{T}_{Ms}$ (MPa/K) | $b^{T}_{Af}$ (MPa/K) | $M_s$ (°C) | $A_f$ (°C) |
| 0.035 | 5 | 5 | -75 | -30 |
| $H_s$ | $\alpha_0$ | $\alpha_1$ | $\alpha_{eps}$ | $n_{surf}$ |
| 10 | 0.05 | 0.05 | 1 | 5 |

### 2.3.2 Numerical simulation of the superelastic behavior of the damper

Due to the symmetric conditions, only a quarter of the damper is modeled. 247 S4R shell elements with 756 degrees of freedom (figure 4(a)) are used. S4R is a 4-node, quadrilateral,

stress/displacement shell element with reduced integration and a large-strain formulation. The external edge is clamped and the normal displacement is imposed on the internal edge. The automatic time increment option in ABAQUS© is used with an initial guess of dividing the

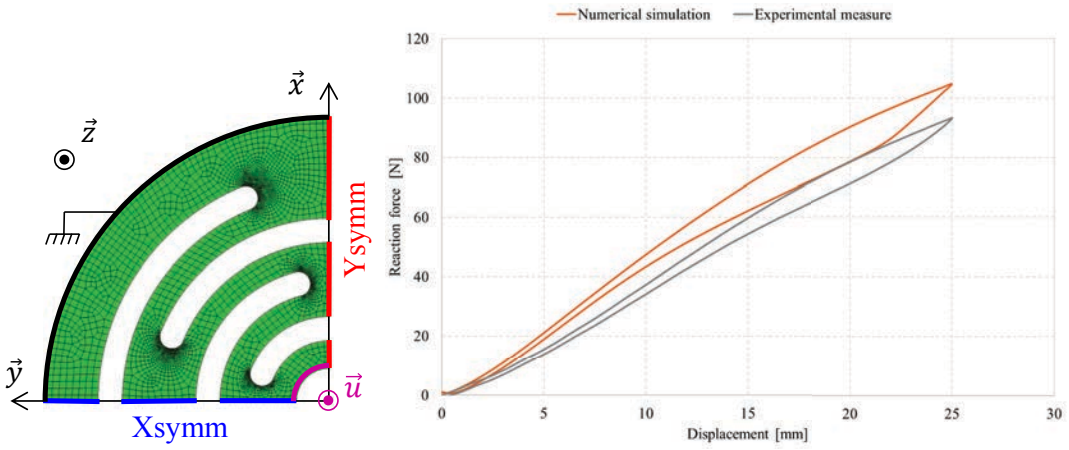


(a) (b)

**Figure 4**: Finite element model of the SMA damper (a) and comparison between the numerical and the experimental responses.

The corresponding experimental cyclic test has been performed on the Zwick/Roell© tensile machine at a quasi static loading rate and at room temperature. The figure 4(b) shows the evolution of the reaction force of the damper versus the imposed displacement. One can notice a good correlation between the experimental and the numerical curves. This result validate the numerical model as a tool to predict the stress and the volume fraction of martensite distributions inside the damper versus the imposed displacement.
This numerical tool is now used to predict the stress, the volume fraction of martensite distributions inside the damper and the required imposed displacement when the forward martensite transformation starts ($\sigma_{VM} = \sigma^{s}_{AM}$) and when the forward martensite transformation finish ($\sigma_{VM} = \sigma^{f}_{AM}$).

The figures 5(a), 5(b) and 5(c), show that the forward martensitic transformation begins in the damper for an imposed displacement about 11 mm. At this statement, there are a localization of the martensite and the maximal von Mises stress at the end of the oblong holes. One can notice the same conclusion at the end of the forward martensitic transformation (figures 5(d), 5(e) and 5(f)) where an imposed displacement about 24 mm is needed. Thus it is clear that for this design of damper, structure effects are preponderant versus the superelastic ones. Furthermore, with an imposed displacement about 24 mm, rotation effects are very important and the fatigue effects due to cyclic solicitations significantly increase through to the break of the damper.

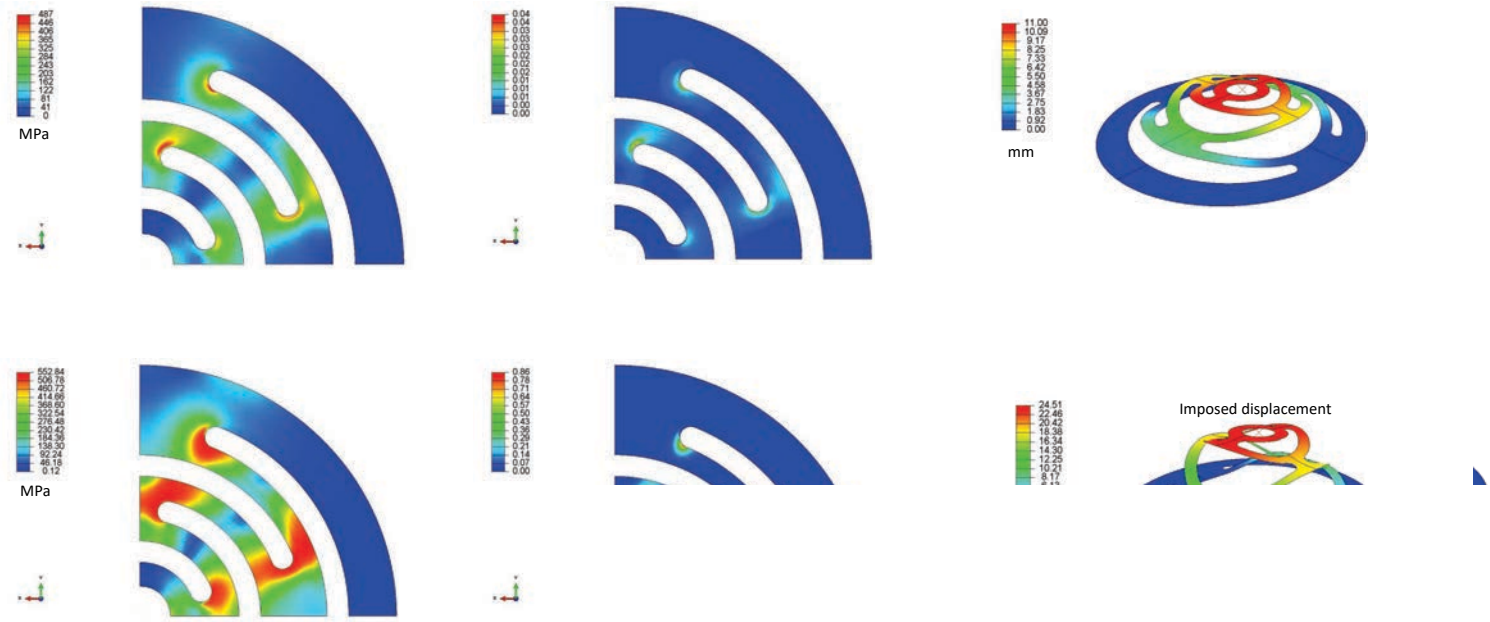


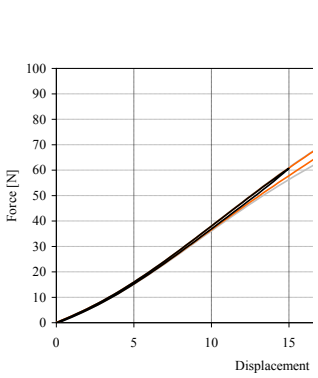


(a)

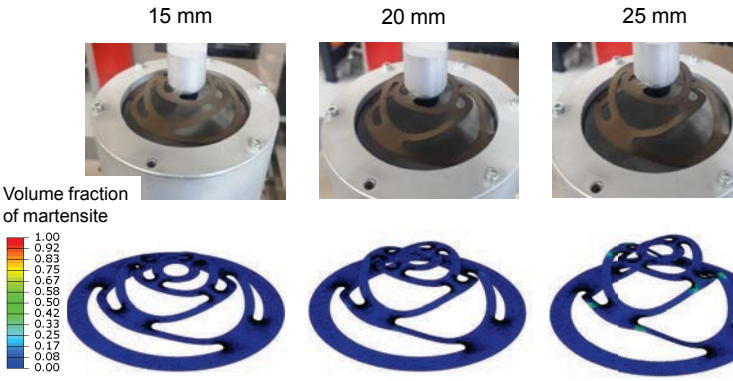


(b)

**Figure 6**: Cylic tensile tests on the damper.

In order to confirm the numerical predictions, cyclic tensile tests are performed with three different displacement amplitudes (15, 20 and 25 mm). The curves given on the figure 6(a) show the evolution of the residual force versus the displacement.
The deformed shape for 15 and 20 mm displacement amplitudes of the disc are given in the figure 6(b) and compared to the numerical simulation.
For each test, a non linear superelastic with hysteresis behavior is shown. Nevertheless, one no-

tice that the hysteresis is essentially zero with a displacement amplitude about 15 mm, moderate with a displacement amplitude about 20 mm and more important with a displacement amplitude about 25 mm. This means that the structure effect is preponderant versus the transformation phase effect, as it is shown on the figure 6(b).that's why we won't imposed an amplitude of displacement above 20 mm during the dynamic tests.

## 3 Dynamical behavior of the damper

The dynamic tensile tests are carried out by Dynamic Mechanical Analysis (DMA). The Zwick/Roell© LTM1 driven by the software TestXpert R© is used here to measure the storage modulus and the loss factor in function of many parameters like the amplitude, the predisplacement, and the frequency.

### 3.1 Equivalent complex stiffness

In order to characterize the damping effect of the structure, the equivalent complex stiffness model based on the Valanis endochronic theory (Valanis [15]) is presented in this section.
At first, one consider a vibrating displacement solicitation of the damper at the pulsation $\omega$ and an amplitude $u_m$ :

$$\tilde{u}(u_m, \omega) = u_m e^{i\omega t} \tag{1}$$

Thus, the reaction force $F$ can be decomposed in Fourier series, and by considering the harmonic balance approximation, written on its first harmonic :

$$\tilde{F}(u_m, \omega) = A(u_m, \omega) e^{(i\omega t + \Phi(u_m, \omega))} \tag{2}$$

where :

$$\begin{aligned} A(u_m, \omega) &= \sqrt{\left(\frac{\omega}{\pi u_m}\int_0^T F(t)cos(\omega t)dt\right)^2 + \left(\frac{\omega}{\pi u_m}\int_0^T F(t)cos(\omega t)dt\right)^2} \\ \Phi(u_m, \omega) &= Arctan\left(\frac{\int_0^T F(t)cos(\omega t)dt}{\int_0^T F(t)cos(\omega t)dt}\right) \end{aligned} \tag{3}$$

The dynamic stiffness $\tilde{K}$ is also defined as the ratio between the complex reaction force $\tilde{F}$ and the complex imposed displacement $\tilde{u}$ :

$$\tilde{K}(u_m, \omega) = \frac{\tilde{F}(u_m, \omega)}{\tilde{u}(u_m, \omega)} \tag{4}$$

Which leads to the explicit expression of the equivalent stiffness :

$$\tilde{K}(u_m, \omega) = K(u_m, \omega)\left(1 + \eta\left(u_m, \omega\right)\right) \tag{5}$$

where $K$ is the storage stiffness and $\eta$ the loss factor. These expressions are respectively :

$$K(u_m,\omega) = \frac{\omega}{\pi u_m}\int_0^T F(t)cos(\omega t)dt \quad (6)$$
$$\eta(u_m,\omega) = \frac{\int_0^T F(t)cos(\omega t)dt}{\int_0^T F(t)cos(\omega t)dt}$$

These two parameters, $K$ and $\eta$ are directly calculated by the software TestXpert R©.

### 3.2 Influence of the frequency and the amplitude

In this section, The dynamic response and the damping effect of the disc are analysed as function of the amplitude of the symmetric vibrations in the range [1-20 mm] and the frequency in the range [1-10 Hz] (figure 7). For the amplitudes less than 10 mm, one notices some perturbations and oscillations on the storage modulus and the loss factor. It can be explained by the fact that the reaction force for this range of amplitude is very low compared to the load sensor capacity (1 kN) and its measurement can be perturbed by some noise. Nevertheless, it is not a problem because the phase transformation and thus the interest of the damper began above the amplitudes of vibration about 10 mm.
In the range [10-20 mm] an increase of the loss factor is notice. It is due to the fact that forward martensitic transformation starts for an amplitude of vibration around 10 mm. Furthermore, an increase of the storage modulus is noticed for an amplitude of vibrations from 10 mm to 15 mm. Above 15 mm, a stabilization of the stiffness is noticed. Thus, it appears that the best performances of the damper are in the range [15 - 20 mm].
For a given amplitude of vibration, an increase of the frequency leads to an increase of the dynamic stiffness and a decrease of the loss factor. Nevertheless the influence of the frequency is

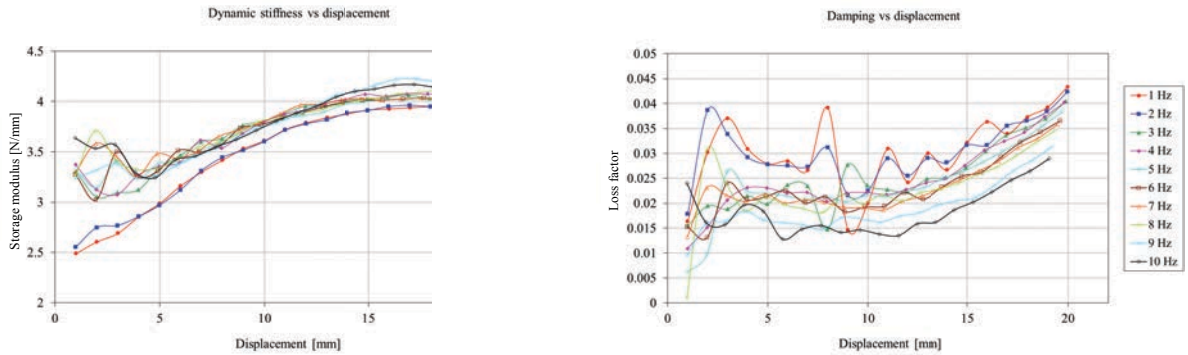


(a) (b)

**Figure 7**: Storage modulus and loss factor versus the amplitude of displacement and the frequency.

### 3.3 Influence of the pre-displacement and the amplitude

The graphs shown on the figure 8 are respectively the storage stiffness and the loss factor, both in function of a pre-displacement in the range [1-10 mm] and the amplitude of vibrations which is in the range of 1 mm around the value of the given pre-displacement. The maximum value of the loss factor - and thus the damping effect - are reached at high values of the pre-displacement and the amplitude of vibrations. These values correspond to maximum forward martensite transformation. Here, the storage stiffness is at its average value.
Thus, in order to get the best damping effect, it's better to have a tension pre-displacement about 10 mm.

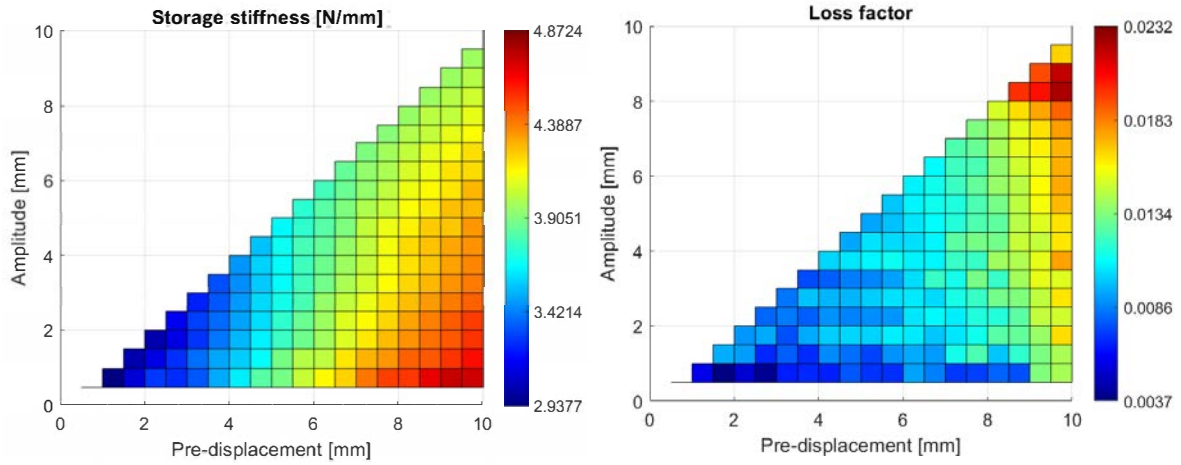


(a) (b)

**Figure 8**: Tensile tests on NiTi tensile samples.

## 4 Conclusion

In this communication, the experimental dynamic mechanical analysis (DMA) of an innovating NiTi holed disc is presented. This investigation leads to characterize the damping effect with the equivalent complex stiffness tool. To do this, a numerical tool using a phenomenological model for the SMA superelastic effect implemented in Abaqus© was designed at first. This numerical tool allows to determine the minimum amplitude of vibrations where the martensitic transformation starts inside the disc and the maximum amplitude of vibrations allowed by the disc to prevent its damage. Thus, in this range of amplitude of vibrations, many parameters such as the frequency, the amplitude of vibrations and the pre-displacement were analysed at room temperature. The results clearly show an optimal set of these parameters which gives the best damping effect of the disc. This work will be continued by studying the effect of the temperature on the damping effect (a cold temperature and a warm one for example). And finally, this experimental database will allow to build a numerical tool to develop and optimize applications

for control in civil engineering.

## REFERENCES

[1] F. Bono and D. Tirelli, "Characterisation of materials for the innovative antiseismic techniques," *JRC ISPRA, Internal report*, 1999.

[2] D. Tirelli, V. Renda, and F. Bono, "Characterisation of shape memory alloys applications to the retrofitting of brick masonry wall by the pseudo-dynamic method and numerical models," *JRC ISPRA, Internal report*, 2000.

[3] M. Dolce, D. Cardone, and R. Marnetto, "Sma recentering devices for seismic isolation of civil structures," *Smart structures and materials 2001: Smart systems for bridges, structures, and highways*, vol. 4330, pp. 238–249, 2001.

[4] M. Piedboeuf, R. Gauvin, and M. Thomas, "Damping behaviour of shape memory alloys: strain amplitude, frequency and temperature effects," *Journal of Sound and Vibration*, vol. 214, no. 5, pp. 885–901, 1998.

[5] C. Fang, X. Zhou, A. I. Osofero, Z. Shu, and M. Corradi, "Superelastic sma belleville washers for seismic resisting applications: experimental study and modelling strategy," *Smart Materials and Structures*, vol. 25, no. 10, p. 105013, 2016.

[6] L. Janke, C. Czaderski, M. Motavalli, and J. Ruth, "Applications of shape memory alloys in civil engineering structures—overview, limits and new ideas," *Materials and Structures*, vol. 38, pp. 578–592, 2005.

[7] F. Gandhi and D. Wolons, "Characterization of the pseudoelastic damping behavior of shape memory alloy wires using complex modulus," *Smart Materials and Structures*, vol. 8, no. 1, p. 49, feb 1999.

[8] M. Collet, E. Foltête, and C. Lexcellent, "Analysis of the behavior of a shape memory alloy beam under dynamical loading," *European Journal of Mechanics-A/Solids*, vol. 20, no. 4, pp. 615–630, 2001.

[9] F. Amarante Dos Santos and C. Cismasiu, "Comparison between two sma constitutive models for seismic applications," *Journal of Vibration and Control*, vol. 16, no. 6, pp. 897–914, 2010.

[10] M. Megdiche, A. Sallami, F. Thiebaud, T. Bouraoui, T. B. Zineb, and S. A. Chirani, "Experimental analysis of the pseudoelastic damping capacity of the fe-30mn-6si-5cr shape memory alloy," *Smart Materials and Structures*, vol. 29, no. 8, p. 084002, 2020.

[11] R. Mirzaeifar, R. DesRoches, and A. Yavari, "A combined analytical, numerical, and experimental study of shape memory alloy helical springs," *International Journal of Solids and Structures*, vol. 48, no. 3-4, pp. 611–624, 2011.

[12] F. Thiebaud and T. Ben Zineb, "Experimental and finite element analysis of superelastic behaviour of shape memory alloy for damping applications," *Mechanics & Industry*, vol. 15, no. 5, pp. 371–376, 2014.

[13] B. Peultier, T. Ben Zineb, and E. Patoor, "Macroscopic constitutive law of shape memory alloy thermomechanical behaviour. application to structure computation by fem," *Mechanics of Materials*, vol. 38, no. 5, pp. 510–524, 2006, shape Memory Alloys.

[14] Y. Chemisky, A. Duval, E. Patoor, and T. Ben Zineb, "Constitutive model for shape memory alloys including phase transformation, martensitic reorientation and twins accommodation," *Mechanics of Materials*, vol. 43, no. 7, pp. 361–376, 2011.

[15] K. Valanis, "A theory of viscoplasticity without a yield surface. part 1. general theory," *Arch. Mech.*, vol. 23, p. 30, 12 1970.